



# Effect of Photoresist Biomimetic Surface Roughness on Droplet Evaporation Dynamics

Zhihao Zhang<sup>1</sup> · Xiangcheng Gao<sup>1</sup> · Yuying Yan<sup>1</sup>

Received: 12 September 2024 / Revised: 17 March 2025 / Accepted: 20 March 2025  
© The Author(s) 2025

## Abstract

Control of the wetting properties of biomimetic functional surfaces is a desired functionality in many applications. In this paper, the photoresist SU-8 was used as fabrication material. A silicon wafer was used as a substrate to prepare a biomimetic surface with different surface roughness and micro-pillars arranged in array morphology. The evaporation dynamics and interfacial heat transfer processes of deionised water droplets on the bioinspired microstructure surface were experimentally studied. The study not only proves the feasibility of preparing hydrophilic biomimetic functional surfaces directly through photoresist materials and photolithography technology but also shows that by adjusting the structural parameters and arrangement of the surface micro-pillar structure, the wettability of the biomimetic surface can be significantly linearly regulated, thereby effectively affecting the heat and mass transfer process at the droplet liquid-vapour interface. Analysis of the results shows that by controlling the biomimetic surface microstructure, the wettability can be enhanced by about 22% at most, the uniformity of the temperature distribution at the liquid-vapour interface can be improved by about 34%, and the average evaporation rate can be increased by about 28%. This study aims to provide some guidance for the research on bionic surface design based on photoresist materials.

**Keywords** Biomimetics · Droplet evaporation · Surface roughness · Wettability · Interfacial phenomenon

## 1 Introduction

Droplet evaporation is ubiquitous daily and essential in many industrial processes [1]. Whether it is the quasi-steady evaporation of sessile droplets or the transient evaporation of droplet impact, the evaporation process is closely related to the surface that the droplets contact. Therefore, the characteristics of the solid surface have a crucial influence on the heat transfer, mass transfer, and even the jumping or movement process of the droplets [2–5]. Based on this, a large amount of research has focused on the design and preparation of solid surfaces, among which surface design based on biomimicry, which is a combination of the Greek words “bios” (meaning life) and “mimesis” (meaning imitation) and generally refers to the study and replication of biological systems [6], has gradually become an essential

means to regulate the dynamic behaviour of droplets [7–9]. Among them, the microstructure of the biomimetic surface significantly affects the wetting and evaporation process of droplets [10]. Therefore, studying the design principles of bionic surface microstructure is of great significance for the in-depth application of bionic surfaces in the fields of phase change heat transfer [11], spray cooling [12], water resources management [13], self-cleaning [14], medical health and environmental protection [15, 16], it also helps to reveal the influencing mechanism of the droplet dynamics [17].

Among the many parameters that affect the morphology of solid surfaces, surface roughness, as a parameter that determines surface texture and flatness, significantly affects the physical and chemical properties of the surface [18]. Naturally, research on the effect of roughness on biomimetic surface properties has also been widely conducted [19]. Yang et al. [20] used 3D printing technology to prepare a bionic hair surface with a bionic eggbeater microstructure based on liquid resin materials. It has enhanced superhydrophobicity function and makes it easier for water droplets to slide off the surface. Li et al. [21] prepared a

✉ Yuying Yan  
yuying.yan@nottingham.ac.uk

<sup>1</sup> Faculty of Engineering, University of Nottingham,  
University Park, Nottingham, UK

super-hydrophobic bionic surface with a honeycomb structure on aluminium alloy. The results showed that as the spacing of the microstructures decreases, the hydrophobicity of the bionic surface also increases. Günay et al. [22] etched silicon pillars on a silicon substrate and then prepared an octafluorocyclobutane ( $C_4F_8$ ) layer on the surface to construct a bionic hydrophobic surface. The results show that the evaporation rate of the droplets and the microscopic wettability pattern are not affected by pillar distance. Besides, Bhushan et al. [23] and Das et al. [24] were inspired by the plant epicuticular wax structure to fabricate a series of biomimetic functional surfaces, and the study comprehensively demonstrated the progressive influence mechanism based on fabrication process, surface roughness and surface wettability. Nosonovsky et al. [25] etched silicon pillars on the substrate and covered them with tetrahydroperfluorodecyltrichlorosilane to prepare a bionic hydrophobic surface. The study found that the droplets' contact angle hysteresis will change as the distance changes. Similarly, bioinspired by red rose petals, Lin et al. [26] etched square micro-pillars on a transparent PDMS substrate to prepare a hydrophobic biomimetic surface. The study found that when the surface roughness increases from 1.0 to 1.93, the wetted state of the droplets will experience a series of changes from Wenzel to Lotus mode. Then, Nosonovsky et al. [27] proposed roughness factor parameters representing changes in surface energy density and the spacing factor that characterises changes in the patterned surface contact area, and they pointed out that these novel parameters can be applied to the design of bionic superhydrophobic surfaces. However, most of these studies on biomimetic surface roughness are based on biomimetic hydrophobic or superhydrophobic surfaces, while studies on biomimetic hydrophilic surfaces are rare.

In addition, regarding the preparation process of bionic surfaces, many studies are based on etching micro-pillar structures to study the impact of surface configuration on the physical and chemical properties of bionic surfaces as well as droplet wettability and heat and mass transfer processes [28]. In this process, different materials will be tried to prepare micro-pillar structures, and the impact of their structural parameters on biomimetic surface properties will be studied [29]. Shahsavan et al. [30] summarised a large number of related studies. They showed that in biomimetic micropatterned surfaces, the low aspect ratio of the surface microstructure will produce superhydrophobicity and low adhesion effects. In contrast, the high aspect ratio will lead to a high adhesion force effect. Liang et al. [31] and Luo et al. [32] were bioinspired by lotus leaves and *Salvinia molesta* leaves, respectively. They prepare a bionic surface with micropillars, which gives it superhydrophobic properties and withstands long-term high temperatures and ultraviolet radiation. Okulova et al. [33] combined nanoglass

and micro-pillar structures to prepare a multi-layered biomimetic functional surface, which could maintain superhydrophobicity for extended periods and be used on flexible substrates. Lee et al. [34] studied the evaporation mode of mixed droplets based on the surface of superhydrophobic silica pillars and discovered the pseudo-CCA evaporation mode. Besides, Hu et al. [35] also studied the impact of pillar height on structured surfaces on impact dynamics based on the numerical simulation method of Volume-of-Fluid (VOF). They found that taller pillars are more conducive to maintaining the Cassie state. Zhang et al. [36] mainly used picosecond laser ablation to prepare a nanopillar microstructure bionic water-transporting surface on a copper substrate, and its superhydrophobicity remained after being placed under natural conditions for 8 months. Similarly, Li et al. [37] also based on copper materials and used wire-cut electric discharge machining to prepare a micro-pillar structure surface. The surface was also made superhydrophobic without chemical modification. Kim et al. [38] based on the ultraviolet light curing method of polyurethane acrylate resin to prepare hydrophobic biomimetic surfaces with various shapes of micro-pillar structures. The research results show that hexagonal and octagonal arrays can achieve better hydrophobicity. At the same time, Nasser et al. [39] used laser-induced methods to use graphene with various structures (cylindrical, hemispherical, and sheet structures) to print biomimetic functional surfaces with superhydrophobic or superhydrophilic properties, and the wettability of the surface is also could be controlled to a precise degree. In addition, Li et al. [40] prepared medical chip surfaces with biomimetic configurations on silicon wafers of medical MEMS based on the fractal principle of the Sierpinski triangle and Sierpinski carpet, and the study found that all of them can improve the hydrophobicity of biomimetic surfaces to different degrees under different conditions. As mentioned above, in addition to numerical simulation methods, the current preparation of surface bionic microstructures is based on common metal or non-metallic materials. In contrast, based on semiconductor and electronic technology, the biomimetic structured surfaces prepared directly based on photoresist materials are rare.

In summary, biomimetic functional surfaces are being increasingly studied due to their broad applicability and unique characteristics [41–43]. However, most of these studies are usually based on achieving super-hydrophobic functions, and there are few studies on conventional hydrophilic biomimetic surfaces. In addition, as an indispensable material in electronic technology, the exploration of directly etching surface microstructures on photoresists and researching wettability and heat and mass transfer characteristics is still relatively sporadic. Therefore, it becomes necessary to research photoresist-based biomimetic functional surfaces.

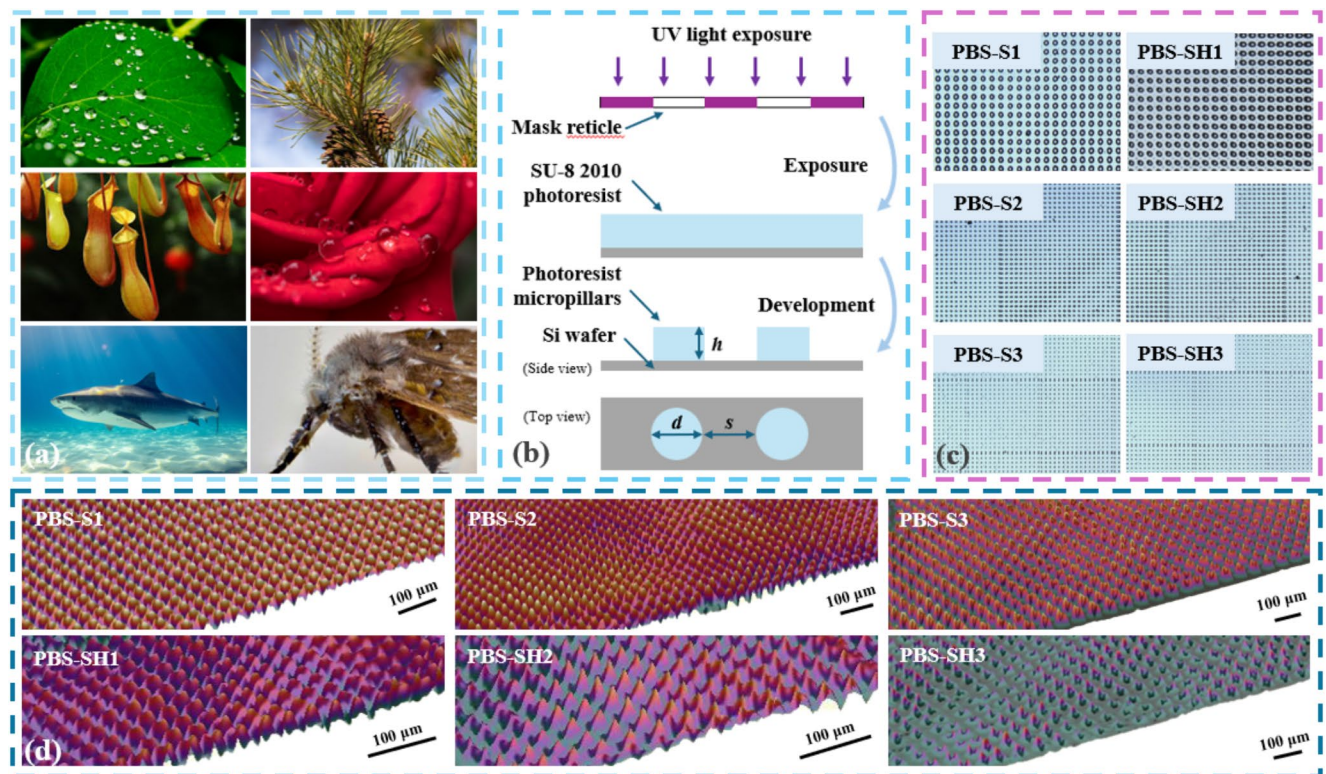
Based on the above, in this paper, SU-8 photoresist was selected to prepare hydrophilic biomimetic surface microstructures, and the surface roughness of the biomimetic surface was regulated by quantitatively controlling the spacing and height of the surface micro-pillars. The first and second sections of this paper introduce the research progress of biomimetic surfaces in related fields and the use of materials, equipment, and surface preparation in this experiment. In the third section, the experimental results are analysed to explore the influence of microstructure on the wettability of bionic surfaces and the heat and mass transfer characteristics of droplet interfaces. The fourth section summarises and presents the research prospects. The study hopes to guide the design, fabrication and application of bionic functional surfaces based on photoresists.

## 2 Materials and Experimental Setup

Bionics is the invention of new science and technology based on the study of the structure and function of organisms. This process is also due to natural species richness and unique biological properties, and some typical examples are shown in Fig. 1 (a). The regular production of microstructures on the surface can maximise the quantitative control of the overall structural parameters of the biomimetic surface,

such as roughness, which is conducive to subsequent research. Therefore, this study selected the method of etching micro-pillars on silicon wafers to realise the production of biomimetic functional surfaces and to carry out research on droplet wetting and heat and mass transfer characteristics. This study used negative photoresists SU-8 2010, which has the advantages of high chemical resistance, temperature resistance and good mechanical stability [44], to fabricate micro-pillars and the specific processing flow and method are shown in Fig. 1 (b). It is worth mentioning that due to the complexity of the micro-pillar processing process, it is difficult to control the height of the micro-pillars with extremely high accuracy. Therefore, in this article, the height of the micro-pillars is characterised by calculating the overall average height. Finally, six types of biomimetic surfaces were fabricated in this study, as shown in Fig. 1 (c). besides, a 3D optical profilometer (KLA Zeta-20 Optical Profiler, United States) also explicitly characterised its surface morphology, as shown in Fig. 1 (d). In this article, some basic data are listed in tables, and the rest are listed in data graphs for intuitive understanding. The specific configuration parameters of these bionic functional surfaces are shown in Table 1.

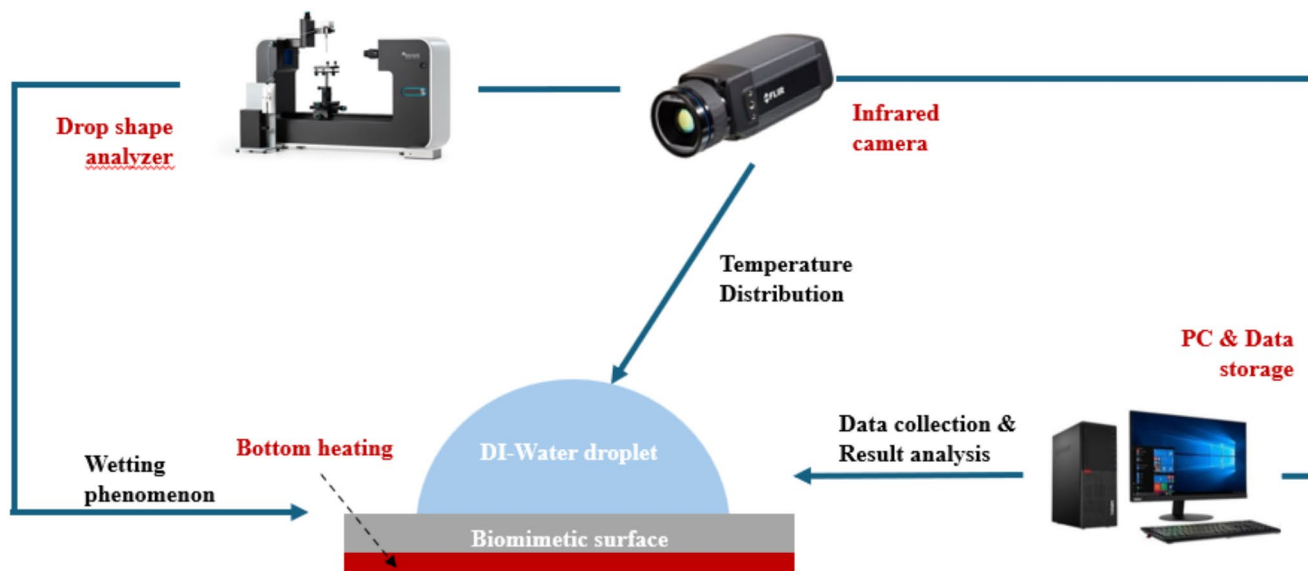
The experimental setup used in this study is shown in Fig. 2. The infrared camera (FLIR A655sc, United States) is used to observe the temperature distribution of the



**Fig. 1** a Plant surfaces or animal skins with unique surface properties in nature; b photoresist micro-pillar preparation process based on photolithography; c different biomimetic surfaces under the microscope; d biomimetic surface profile measured by an optical profilometer

**Table 1** Parameters of biomimetic surface photoresist micro-pillars

	PBS-S1	PBS-S2	PBS-S3	PBS-SH1	PBS-SH2	PBS-SH3
Spacing $s$ ( $\mu\text{m}$ )	15	20	40	15	20	40
Diameter $d$ ( $\mu\text{m}$ )	20	20	20	20	20	20
Average height $h$ ( $\mu\text{m}$ )	50	50	50	40	40	25
Roughness factor $r$	3.565	2.963	1.873	3.052	2.571	1.436

**Fig. 2** Experimental process and equipment schematic diagram**Table 2** Some physical properties of the deionized water under the condition of 60°C

	Density	Viscosity	Heat capacity	Surface Tension
DI water	0.98321 g/cm <sup>3</sup>	0.4688 mPa·s	4.1843 J/(g·K)	66.18 mN/m

Deionised water (DI water) liquid-vapour interface. The droplet shape analyser (Biolin Theta Flex, Sweden) measures the shape change of the droplet. At the same time, the prepared biomimetic surface is placed on a temperature-controlled aluminium heating plate. The bottom temperature of this experiment is controlled at 60 °C. The silicon substrate of the biomimetic surface and the heating plate are connected and fixed with silicone grease (RS PRO, UK), which can reduce the contact thermal resistance and maximise the heating effect of the substrate. A pipette (Eppendorf Research plus, Germany) was used to manipulate the droplets during the experiment. The ambient temperature of each test in the laboratory was controlled between 21 °C and 25 °C, and the relative humidity was controlled between 50% and 60%. Since the substrate will have a heating effect on the droplets in the experiment, and considering the simplification of the calculation, this study will be carried out based on the thermophysical parameters of water at 60 °C, and the specific parameters are shown in Table 2.

Besides, the droplet wetting study is mainly divided into the Wenzel state and the Cassie-Baxter state, and the Wenzel state equation could be defined as [45]:

$$\cos\theta_m = r\cos\theta_Y \quad (1)$$

and the roughness factor  $r$  in this study could be defined as:

$$r = \frac{(d+s)^2 + \pi \cdot d \cdot h}{(d+s)^2} \quad (2)$$

At the same time, the adhesion work is defined based on the Dupré equation [46] can be described as:

$$W_{AB} = Y_A + Y_B - Y_{AB} \quad (3)$$

where A and B mean phase or object, when the two objects are solid and liquid, respectively, the work of adhesion can also be described as:

$$W_{SL} = \sigma_S + \sigma_L - \sigma_{SL} \quad (4)$$

where  $\sigma_S$  means surface free energy,  $\sigma_L$  means surface tension of liquid, and  $\sigma_{SL}$  means interfacial tension between solid and liquid phase. Then, the simplified work of adhesion per unit area could be described as:

$$W_{PSL} = W_{SL}/A \quad (5)$$

where  $A$  is defined as the two-dimensional contact area of the liquid-vapour interface. Meanwhile, the average evaporation rate  $E_{avg}$  is defined as:

$$E_{avg} = M_0/T_{total} \quad (6)$$

$$M_0 = \rho_0 \cdot V_0 \quad (7)$$

where  $M_0$  and  $V_0$  are the initial mass and volume of the droplet, respectively.  $T_{total}$  is the total evaporation time, and  $\rho_0$  is the DI water density at 60°C.

### 3 Results and Discussion

#### 3.1 Effect of Biomimetic Surface Pillar Arrangement on Droplet Wetting Properties

For biomimetic surfaces, the wettability has always been of excellent research significance. Therefore, this paper first studied the wettability of biomimetic surfaces under different roughness conditions. The changes in the Contact Angle (CA) and dimensionless Contact Line (CL) with time when the droplet volume is 0.25, 0.5, 0.75 and 1.0  $\mu\text{L}$ , respectively, are shown in Fig. 3 (a-d). It is worth noting that the change of the dimensionless contact line is expressed as  $D/D_0$ , where  $D_0$  is the contact diameter of the droplet in the initial equilibrium state and  $D$  is the contact diameter in the real-time state. First, as shown in Fig. 3 (a), when a 0.25  $\mu\text{L}$  DI water droplet evaporates on the three kinds of biomimetic surfaces, the initial contact angle increases by about 15% as the roughness increases. At the same time, the contact line of the droplet also shows the same change trend. In the initial stage of droplet evaporation, the contact line is in a pinned state. As the evaporation process proceeds, approximately in the middle and later period of the overall evaporation process, the contact line of the droplet begins to move and shrink until the end of evaporation, with an overall shrinkage of about 20-30%. It can also be seen from this that the evaporation mode of the droplet goes through a constant contact radius (CCR) mode in the first half, where the contact radius remains unchanged while the contact angle continues to decrease, and a mixed evaporation mode in the second half where both the contact angle and the contact line decrease simultaneously. At the same time, as shown in Fig. 3, the change trends of the droplet's contact angle and contact line remain roughly the same when the droplet volume increases. As a biomimetic surface with overall hydrophilicity, when its surface roughness increases, regardless of the size of the droplet volume, it will increase its surface

wettability. This phenomenon is consistent with the description of the Wenzel equation, as shown in Eq. (1). Besides, the biomimetic surface will also impact the change of the droplet evaporation mode. As the roughness decreases, the time point of evaporation mode changes from CCR to mixed will also be later due to the increase in roughness delaying the time point when the surface tension of the liquid-vapour interface reaches the depinning force of the contact line.

At the same time, under different droplet volume conditions, the changes in the work of adhesion between the three biomimetic surfaces of PBS-S1, PBS-S2, and PBS-S3 and the DI water droplets are shown in Fig. 4 (a-d). It is worth mentioning that the work of adhesion, as an essential concept in interfacial physical chemistry, is of great significance in describing the characteristics of interfaces. Assuming that the surfaces of two immiscible objects are in contact with each other, the physical meaning of adhesion work is the work required to separate the two objects [47]. This paper uses the simplified per unit area work of adhesion ( $W_{PSL}$ ) for description, and the specific calculation principle is shown in Eqs. (3–5). Taking 0.25  $\mu\text{L}$  of DI water as an example, as shown in Fig. 4 (a), the work of adhesion between the droplet and the biomimetic surface decreases as the roughness declines, and the adhesion work of the liquid-solid interface decreases by about 17% when the surface changes from PBS-S1 to PBS-S3. At the same time, with the droplet volume increase from 0.25  $\mu\text{L}$  to 1.0  $\mu\text{L}$ , the changing trend of the work of adhesion remains consistent. That is, the influence of the change of the biomimetic surface roughness on the change of the adhesion work will not change with the change of the droplet volume. This is because the work of adhesion is one of the biomimetic surface properties, and the biomimetic surface microstructures play a dominant role in it by changing the wettability. Besides, the variation trend of the dimensionless height ( $H/H_0$ ) of the droplet is also shown in Fig. 4 (a-d), where  $H_0$  is the initial height of the droplet, and  $H$  is the real-time height of the droplet. As the surface roughness increases, the rate of change of the dimensionless droplet height also increases, and this trend is not affected by the droplet volume. This can also be attributed to the increase in roughness, which enhances the mass transfer rate at the droplet liquid-vapour interface.

#### 3.2 Effect of Biomimetic Surface Pillar Height on Droplet Wetting Properties

In the above, we describe how to change the roughness of the biomimetic surface by changing the micro-pillar spacing and then explore its effect on wettability. In this section, based on the same spacing arrangement, the height of the micro-pillars is changed to study the effect of the change in their roughness on the wettability of the biomimetic

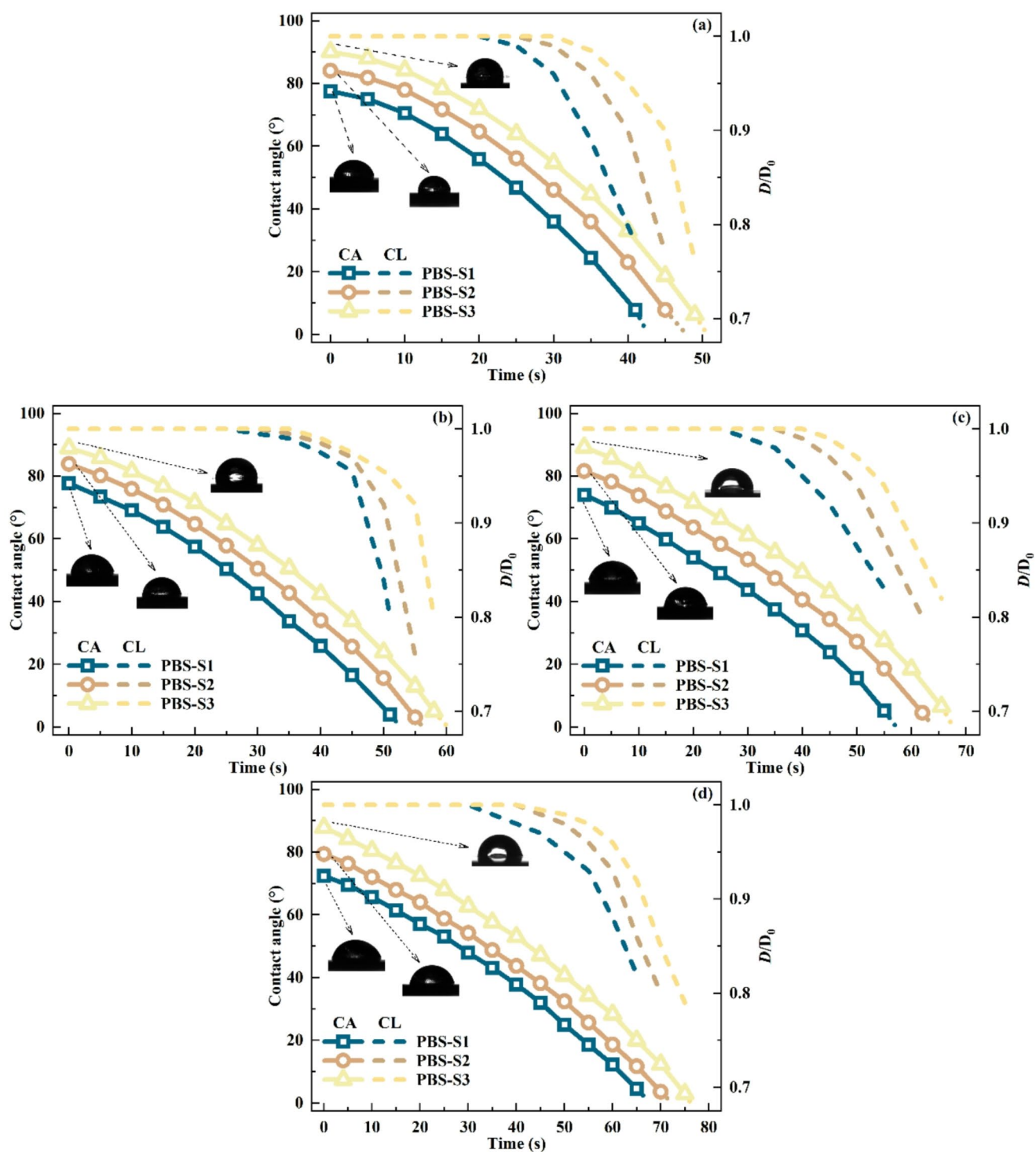


**Fig. 3** Changes of contact angle and dimensionless contact diameter of **a** 0.25  $\mu\text{L}$ ; **b** 0.5  $\mu\text{L}$ ; **c** 0.75  $\mu\text{L}$ ; **d** 1.0  $\mu\text{L}$  DI water droplet on biomimetic surfaces over time

surface. After changing the height, the biomimetic surfaces are named PBS-SH1, PBS-SH2 and PBS-SH3, respectively. The wetting phenomenon and evaporation characteristics of the DI water droplets on these biomimetic surfaces are shown in Fig. 5 (a-d). As shown in Fig. 5 (a), when the

volume of the droplet is 0.25  $\mu\text{L}$ , as the surface roughness of the droplet increases, the contact angle declines by about 13%. The evaporation mode of the droplets still undergoes a transition from the CCR mode to the mixed mode. As the roughness decreases, the time node of the droplet

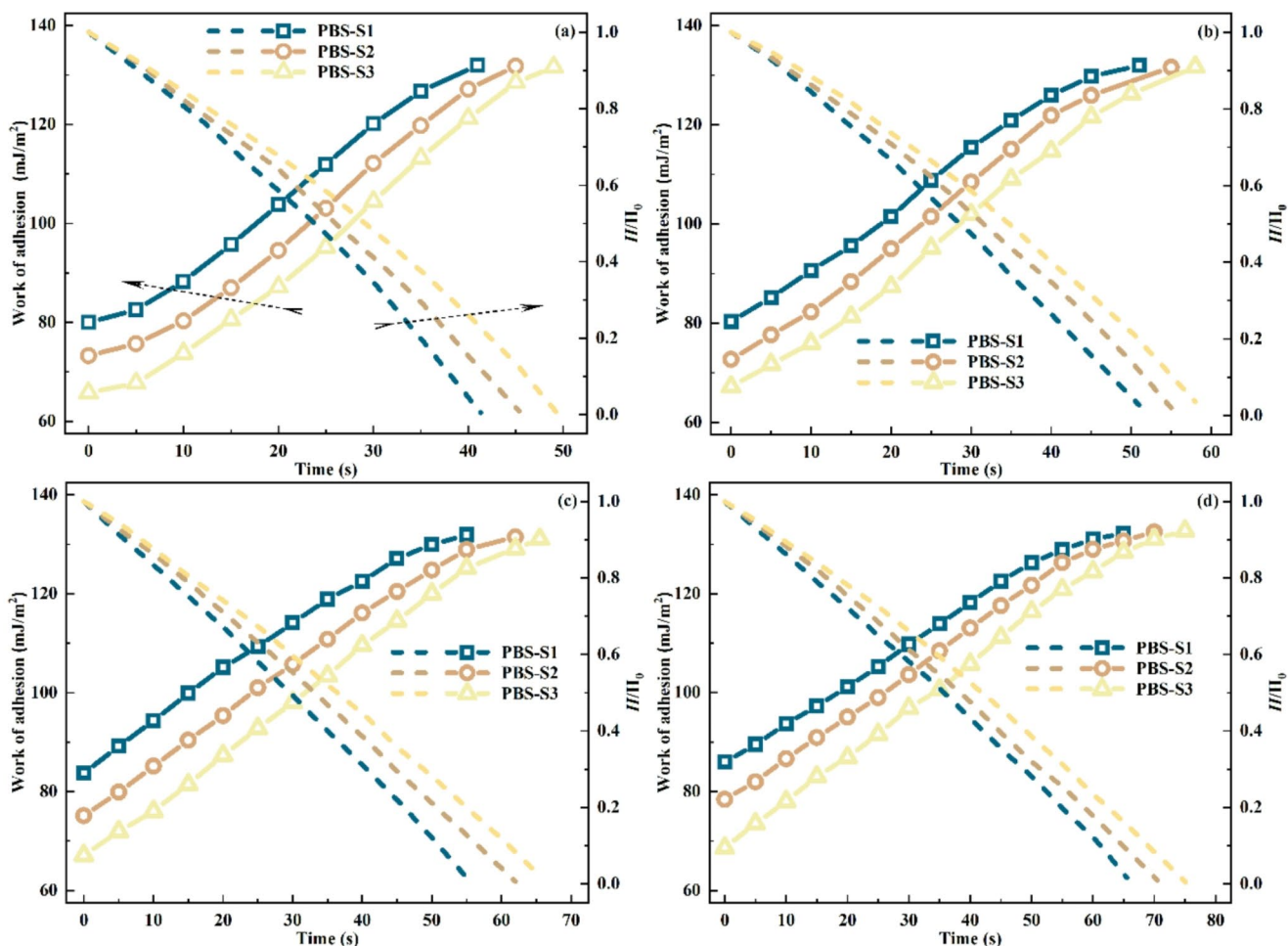


**Fig. 4** Variation of work of adhesion ( $W_{PLS}$ ) with **a** 0.25  $\mu\text{L}$ ; **b** 0.5  $\mu\text{L}$ ; **c** 0.75  $\mu\text{L}$ ; **d** 1.0  $\mu\text{L}$  DI water droplets on different biomimetic surfaces over time

evaporation mode transition is also delayed. At the same time, when the droplet volume increases to 0.5  $\mu\text{L}$ , 0.75  $\mu\text{L}$ , and 1.0  $\mu\text{L}$ , it can be seen from Fig. 5 (b-d) that the change trends of the wetting characteristics on the biomimetic surface remain unchanged. And the evaporation process of the droplet also goes through the two modes of CCR and mixed. In summary, when the roughness of the biomimetic surface is controlled by changing the height of the micro-pillars, the evaporation process of the DI water droplets still follows the same change law described before. It can also be seen that the change in the height of the micro-pillars has no noticeable effect on the transformation of the evaporation mode. The change in surface roughness still has the dominant influence on the evaporation process of droplets.

At the same time, after the height of the micro-pillar structure on the biomimetic surface changes, the work of adhesion between the droplet and the biomimetic surface is shown in Fig. 6 (a-d). As shown in Fig. 6 (a), when a 0.25  $\mu\text{L}$  DI water droplet was placed on the PBS-SH1 surface, its initial work of adhesion was about 76  $\text{mJ}/\text{m}^2$ . In contrast,

when the droplet was placed on the PBS-SH2 and PBS-SH3 surfaces, the work of adhesion decreased to about 69 and 62  $\text{mJ}/\text{m}^2$ , respectively, also reduced by about 10% and 18%, respectively. This can be attributed to the fact that as the roughness of the biomimetic surface decreases, the wettability of the biomimetic surface also weakens, reducing the work of adhesion at the solid-liquid interface of the droplet. At the same time, as the droplet volume increases from 0.25  $\mu\text{L}$  to 1.0  $\mu\text{L}$ , as shown in Fig. 6 (b-d), on these three kinds of biomimetic surfaces, the work of adhesion between the droplet and the surface keeps following a trend of gradually increasing as the evaporation process proceeds. As the evaporation reaches the final phase, no matter on what kind of surface, the work of adhesion between the droplet of each volume and the biomimetic surface will approach about 132  $\text{mJ}/\text{m}^2$ , which is jointly determined by the biomimetic surface characteristics and the physical properties of DI water. The most significant difference is that the work of adhesion on the PBS-SH3 surface always reaches the constant value

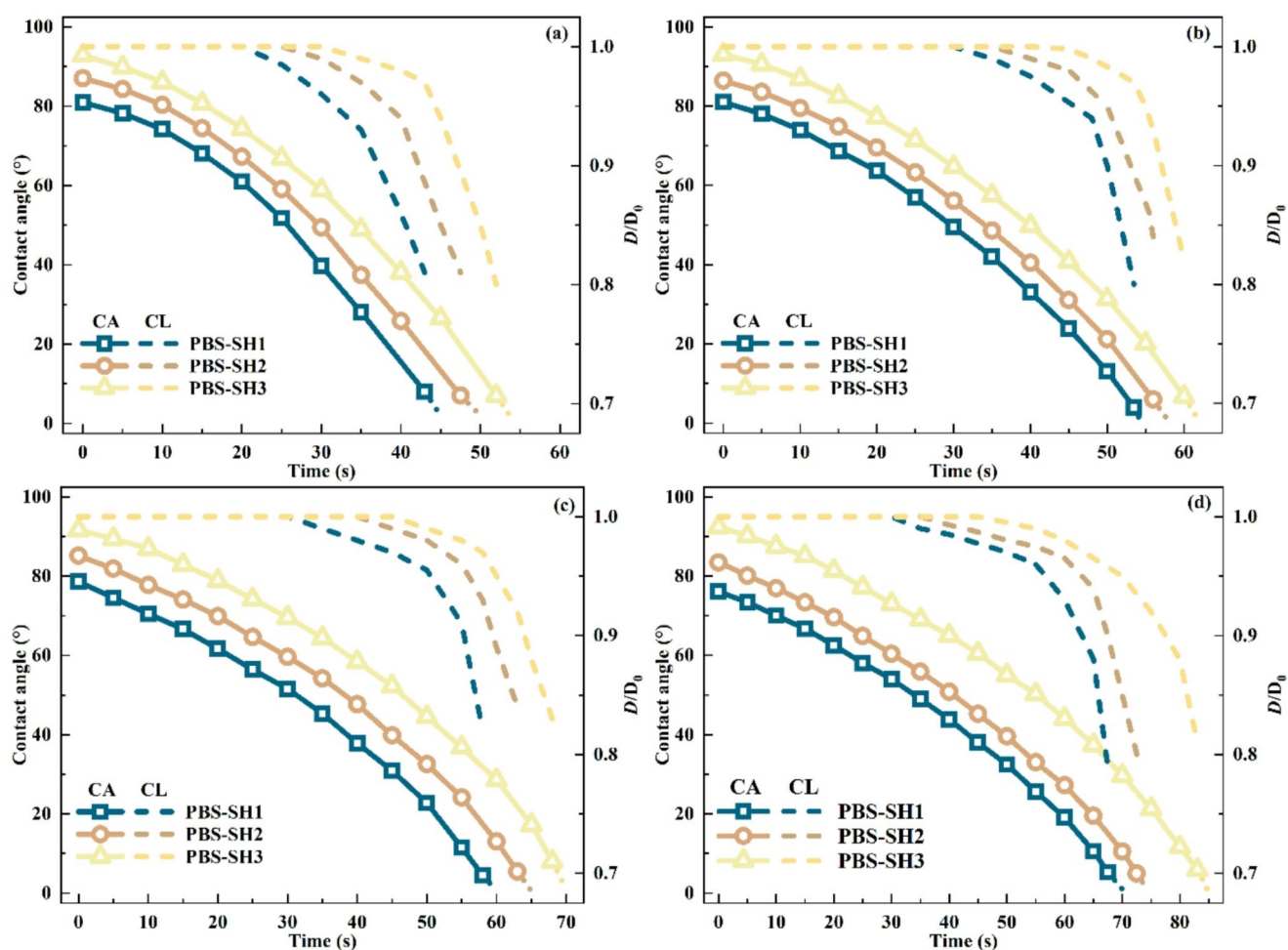


**Fig. 5** Changes of contact angle and dimensionless contact diameter of **a** 0.25  $\mu\text{L}$ ; **b** 0.5  $\mu\text{L}$ ; **c** 0.75  $\mu\text{L}$ ; **d** 1.0  $\mu\text{L}$  DI water droplet on biomimetic surfaces over time

at the latest, which can be attributed to its surface having the worst hydrophilicity.

In addition, to comprehensively compare the effects of biomimetic surfaces of various structures on the wetting characteristics of droplets with different volumes, the changes in the initial equilibrium angle of the droplet with surface parameters were sorted out, as shown in Fig. 7 (a). As seen in Fig. 7 (a), the initial equilibrium contact angle of the droplet is linearly related to the roughness of the biomimetic surface. That is, as the surface roughness increases, the contact angle of the droplet declines. For example, when the droplet volume is 0.25  $\mu\text{L}$ , as the roughness increases, the contact angle can decline from about  $93^\circ$  to about  $77^\circ$ , a reduction of about 17%. At the same time, it can also be seen from Fig. 7 (a) that when the volume of the droplet increases to 0.5  $\mu\text{L}$ , 0.75  $\mu\text{L}$ , and 1.0  $\mu\text{L}$ , respectively, the maximum decrease in the initial equilibrium contact angle of the droplet can also reach 16%, 19%, and 22%, respectively. The reason for this phenomenon can be attributed to the different sizes and arrangements of the micro-pillar

structures on the biomimetic surface, which will significantly change the overall surface roughness and then, based on the Wenzel state of the droplet, will have a crucial impact on the wettability of the biomimetic surface and the apparent contact angle of the droplet. At the same time, the droplet volume also has a minor effect on the initial equilibrium contact angle. For example, on the PBS-SH3 surface, the initial equilibrium contact angle does not change significantly when the droplet volume increases from 0.25  $\mu\text{L}$  to 0.5  $\mu\text{L}$  but decreases by about 5% when the volume increases to 1.0  $\mu\text{L}$ . The reason for this phenomenon is the same as described before. It has nothing to do with the wettability of the biomimetic surface but mainly depends on the effect of gravity. Therefore, the larger the droplet volume, the more pronounced the gravity effect (overcoming the surface tension of the liquid-vapour interface), and the more significant the reduction in the contact angle. In addition, based on the series of biomimetic surfaces, the variation in the magnitude of the adhesion work of DI water droplets with different volumes is shown in Fig. 7 (b). Like the initial

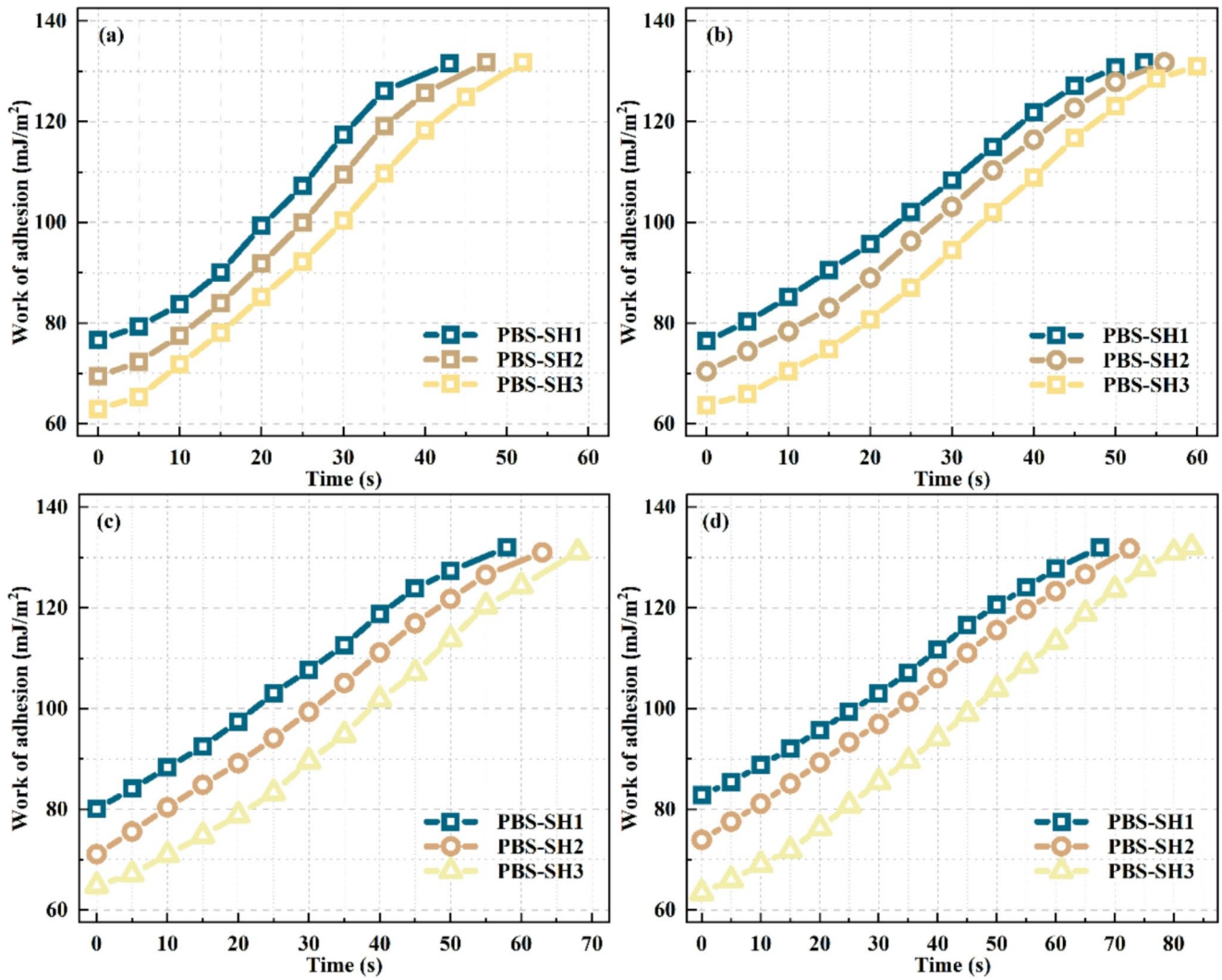


Fig. 6 Variation of work of adhesion (WPLS) with a 0.25 µL; b 0.5 µL; c 0.75 µL; d 1.0 µL DI water droplets on different biomimetic surfaces over time

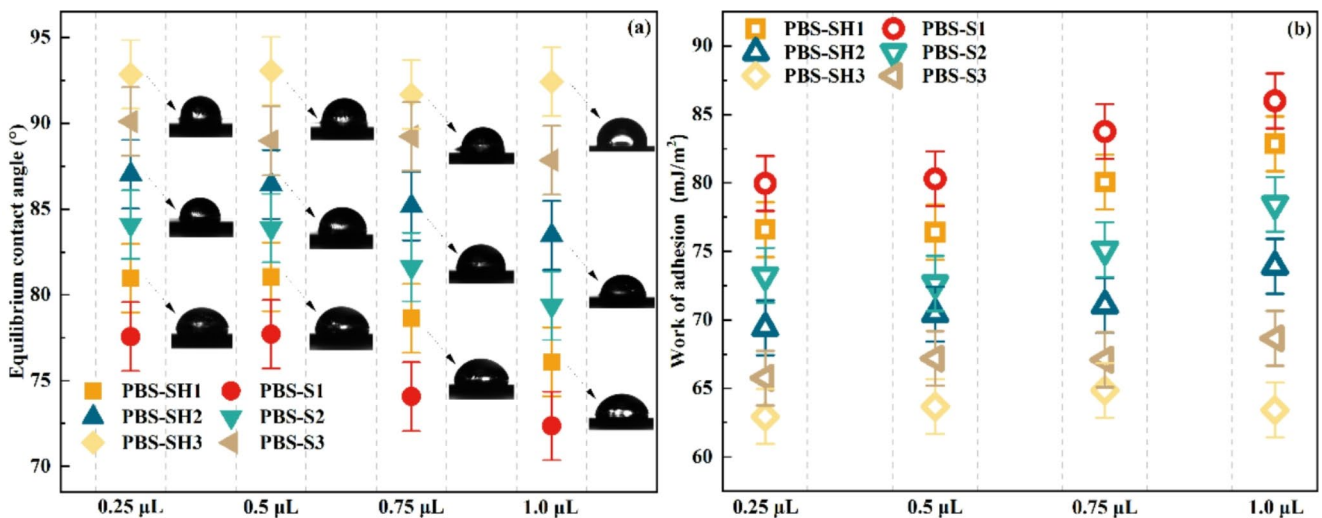


Fig. 7 a Changes in the initial equilibrium contact angles of droplets of different volumes on biomimetic surfaces with roughness degrees; b the work of adhesion corresponding to different initial equilibrium contact angles

equilibrium contact angle, the initial adhesion work also shows an apparent linear relationship with the roughness of the biomimetic surface. The more significant the surface roughness, the greater the work of adhesion, and the maximum increase is approximately 23%.

### 3.3 Effect of Biomimetic Surface Roughness on Droplet Interfacial Heat Transfer Process

The previous mainly introduced the effects of biomimetic surfaces with a series of microstructures on the wetting characteristics of DI water droplets. In addition to the wetting state of the liquid-solid interface, different biomimetic surfaces will also significantly impact the heat and mass transfer process at the liquid-vapour interface of the droplets, which will be discussed in this section. Firstly, the temperature difference  $\Delta T$  between the droplet centre area and the contact line area is defined. It can be used to describe the strength of the evaporative cooling effect, which is usually

caused by evaporation from the interface [48]. At the same time, Fig. 8 (a-d) shows that  $\Delta T$  will also change under different biomimetic surfaces. As the surface roughness increases, the  $\Delta T$  of the droplet will decrease significantly. For example, when a 0.25  $\mu\text{L}$  DI water droplet evaporates on the biomimetic surface, as shown in Fig. 8 (a). When the droplet is placed on the PBS-SH3 surface,  $\Delta T$  is about 4.8  $^{\circ}\text{C}$ . In contrast, when the droplet is placed on the PBS-S3 and PBS-SH1 surface,  $\Delta T$  is about 4.6  $^{\circ}\text{C}$  and 4  $^{\circ}\text{C}$ , which decreases by about 4% and 17%, respectively. This phenomenon can be attributed to the fact that when the roughness of the biomimetic surface increases, the surface wettability is enhanced. The contact angle of the droplet is reduced, which enhances the heat transfer process inside the droplet and improves the temperature uniformity of the liquid-vapour interface while also inhibiting the evaporative cooling effect of the liquid-vapour interface. At the same time, at the initial equilibrium moment of the droplet, the infrared thermal images of a 0.25  $\mu\text{L}$  droplet on different

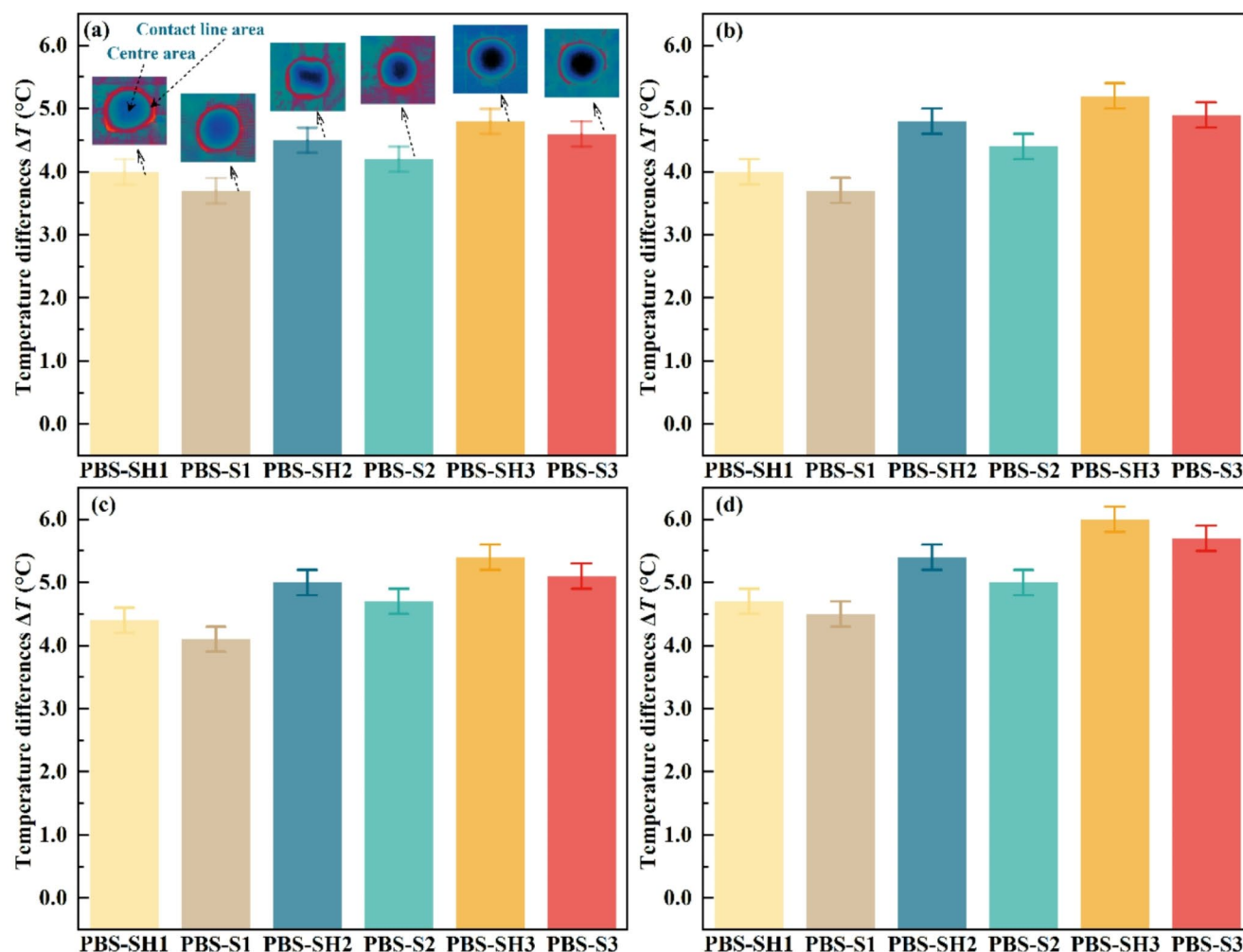


**Fig. 8** The temperature difference between the central and contact line region of **a** 0.25  $\mu\text{L}$ ; **b** 0.5  $\mu\text{L}$ ; **c** 0.75  $\mu\text{L}$ ; **d** 1.0  $\mu\text{L}$  droplet on different biomimetic surfaces

biomimetic surfaces are shown in the inset of Fig. 8 (a). The liquid-vapour interface of the droplet has a pronounced evaporative cooling effect at the initial moment and produces an apparent temperature gradient distribution. Afterwards, as shown in Fig. 8 (b-d), when the droplet volume increases from 0.25  $\mu\text{L}$  to 1.0  $\mu\text{L}$ , the  $\Delta T$  change trend of the liquid-vapour interface remains unchanged, which maintains a linear relationship with the roughness degree. Under various droplet volume conditions, the  $\Delta T$  difference between the PBS-S1 and PBS-SH3 surfaces can vary by 34%.

Meanwhile, the temperature distribution of the droplet liquid-vapour interface changes with time, as shown in Fig. 9, where  $t_{\text{total}}$  refers to the total evaporation time of droplet. Figure 9 (a) and (b) show the evaporation process of a 0.5  $\mu\text{L}$  DI water droplet on the PBS-SH3 and PBS-S3 surfaces, respectively. As the evaporation process proceeds, the temperature distribution at the droplet liquid-vapour interface tends to be uniform. This can be attributed to the dual effects of enhanced thermal conductivity inside the droplet and weakened evaporative cooling effect on the interface. It can also be seen that at the same time point, the temperature distribution inhomogeneity at the droplet liquid-vapour interface on the PBS-SH3 surface is more evident in the early stage. In contrast, the difference in temperature distribution between the two surfaces is not significant in the later stage.

In addition, different biomimetic surfaces will also affect the mass transfer process, which will significantly impact the evaporation rate of droplets. As shown in Fig. 10 (a-d), the average evaporation rate of the droplet during the entire evaporation process is aggregated, which is defined as

Eqs. (6–7), showing the effect of different biomimetic surfaces on the evaporation rate. It can be seen from Fig. 10 (a) that as the biomimetic surface roughness increases, the sessile droplet average evaporation rate also rises. For example, when the droplet is converted from the PBS-SH3 surface to the PBS-S1 surface, the average evaporation rate increases from  $4.73 \times 10^{-3}$  g/s to  $6.0 \times 10^{-3}$  g/s, improving about 27%. Meanwhile, when the droplet volume increases from 0.25  $\mu\text{L}$  to 1.0  $\mu\text{L}$ , the average evaporation rate of the droplet on different biomimetic surfaces is shown in Fig. 10 (b-d). At the same time, when the droplet volume increases from 0.25  $\mu\text{L}$  to 1.0  $\mu\text{L}$ , the average evaporation rate of the droplet on different biomimetic surfaces is shown in Fig. 10 (b-d). The change in the droplet volume does not affect the trend of the average evaporation rate. When the droplet volume is 0.5  $\mu\text{L}$ , 0.75  $\mu\text{L}$  and 1.0  $\mu\text{L}$ , the maximum increase in the average evaporation rate is 17%, 28% and 17%, respectively.

## 4 Conclusion

In this study, the bioinspired micro-pillar structures were fabricated on a silicon wafer based on a photoresist material SU-8. The biomimetic surface roughness was precisely controlled by adjusting the size and arrangement of the micro-pillars. Firstly, two evaporation modes, CCR and mixed, were observed during the evaporation process. At the same time, the changing trend of the work of adhesion between the biomimetic surfaces with different microstructures is also different. The smaller the roughness, the lower the adhesion work for droplets of the same volume. After that, this study also adjusted the micro-pillar average height at

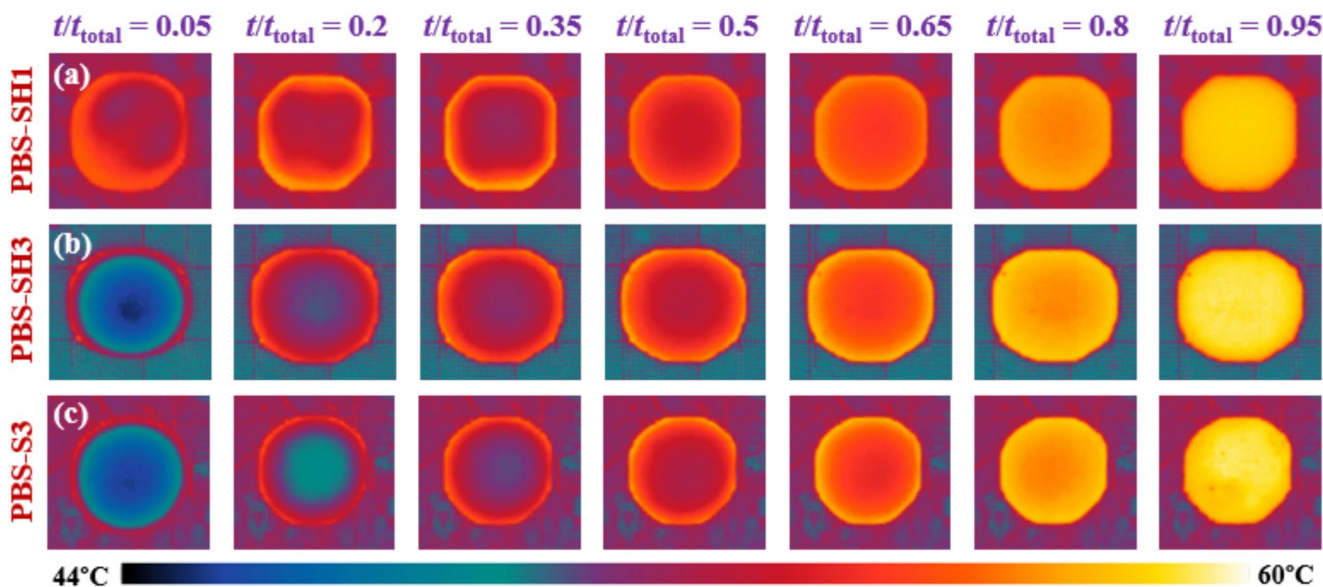


**Fig. 9** Evolution of the temperature distribution at the liquid-vapour interface of a 0.5  $\mu\text{L}$  droplet on the a PBS-SH1, b PBS-SH3, and c PBS-S3 surfaces

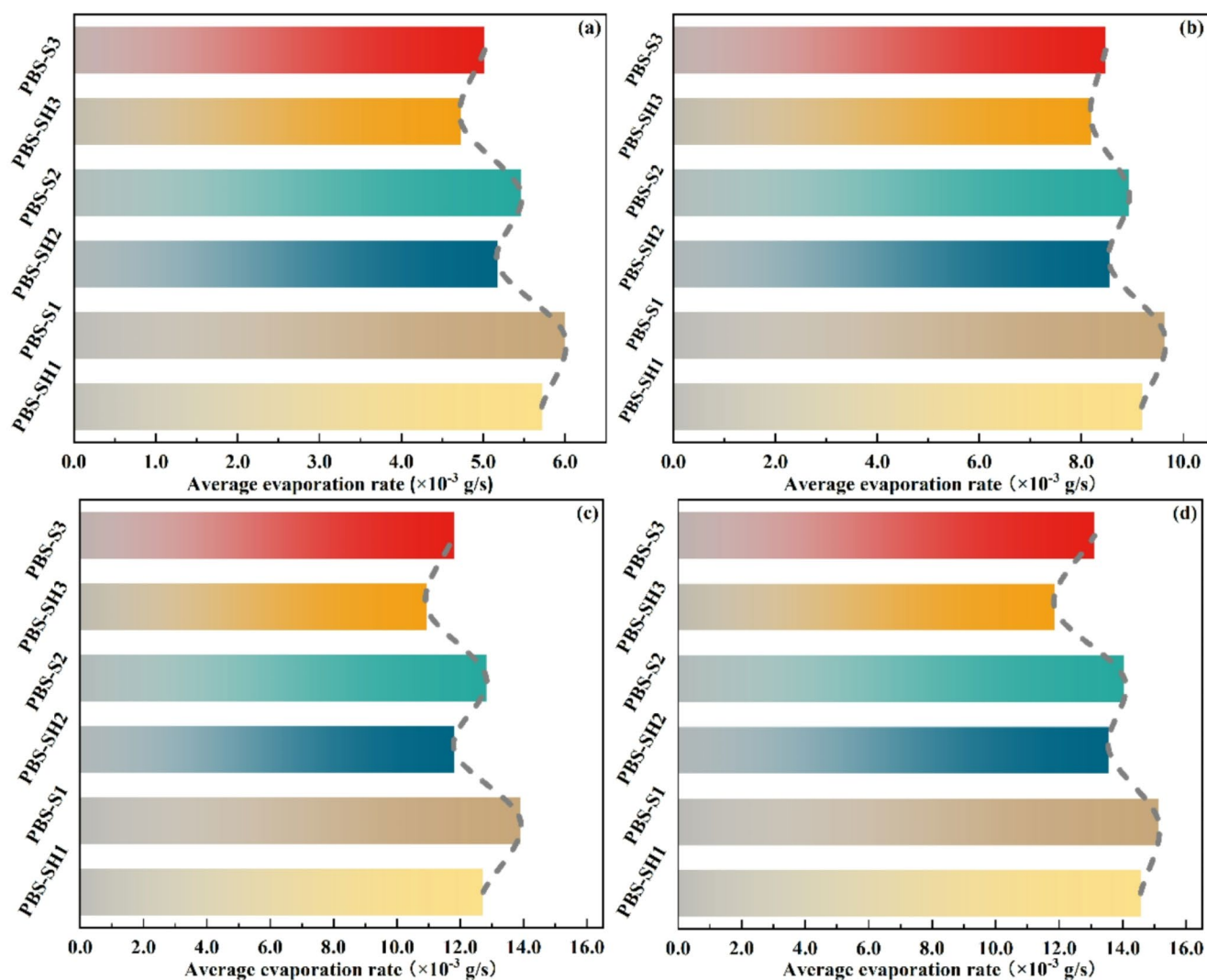


**Fig. 10** Average evaporation rate of **a** 0.25  $\mu$ L; **b** 0.5  $\mu$ L; **c** 0.75  $\mu$ L; **d** 1.0  $\mu$ L droplet located on different biomimetic surfaces

the corresponding spacing, which adjusted the biomimetic surface wettability. Considering the effects of the micro-pillar spacing and height, the results show that as the surface roughness increases, the contact angle can be reduced by up to 22%. When the roughness is reduced to a certain extent, the biomimetic surface can also be transformed into weakly hydrophobic. During the evaporation process, an apparent evaporative cooling phenomenon will occur at the liquid-vapour interface, and it will become more evident as the roughness increases. The temperature difference between different surfaces can be increased by up to 34% on average. At the same time, this phenomenon will also inhibit the overall average evaporation rate by up to 28%. This study demonstrates the feasibility of preparing biomimetic surfaces based on the photoresist, which is expected to help expand the application of biomimetic surfaces in manufacturing electronic devices, oil-water separation, mist collection, and droplet/bubble manipulation.

**Acknowledgements** This work was supported by H2020-MSCA-RISE-778104-ThermaSMART, Royal Society (IEC\NSFC\211210) and doctoral degree scholarship of China Scholarship Council (CSC).

**Authors' Contributions** Zhihao Zhang: Conceptualization, Analysis, Investigation, Data recording & analysis, Validation, Writing—original draft and Revision. Xiangcheng Gao: Data recording and analysis. Yuying Yan: Conceptualisation, Analysis, Investigation, Supervision, Funding acquisition, Writing—review & editing.

**Data Availability** Declaration.

The data that support the findings of this study are available on request from the corresponding author upon reasonable request.

## Declarations

**Conflict of Interest** The authors declare that they have no known competing financial interests or personal relationships that could have appeared to influence the work reported in this paper.

**Open Access** This article is licensed under a Creative Commons Attribution 4.0 International License, which permits use, sharing,

adaptation, distribution and reproduction in any medium or format, as long as you give appropriate credit to the original author(s) and the source, provide a link to the Creative Commons licence, and indicate if changes were made. The images or other third party material in this article are included in the article's Creative Commons licence, unless indicated otherwise in a credit line to the material. If material is not included in the article's Creative Commons licence and your intended use is not permitted by statutory regulation or exceeds the permitted use, you will need to obtain permission directly from the copyright holder. To view a copy of this licence, visit <http://creativecommons.org/licenses/by/4.0/>.

## References

- Zang, D. Y., Tarafdar, S., Tarasevich, Y. Y., Choudhury, M. D., & Dutta, T. (2019). Evaporation of a droplet: From physics to applications. *Physics Reports*, *804*, 1–56. <https://doi.org/10.1016/j.physrep.2019.01.008>
- Malinowski, R., Parkin, I. P., & Volpe, G. (2020). Advances towards programmable droplet transport on solid surfaces and its applications. *Chemical Society Reviews*, *49*(22), 7879–7892. <https://doi.org/10.1039/D0CS00268B>
- Misyura, S., Kuznetsov, G., Volkov, R., & Morozov, V. (2020). Droplet evaporation on a structured surface: The role of near wall vortices in heat and mass transfer. *International Journal of Heat and Mass Transfer*, *148*, 119126. <https://doi.org/10.1016/j.ijheatmasstransfer.2019.119126>
- Benther, J. D., Pelaez-Restrepo, J., Stanley, C., & Rosengarten, G. (2021). Heat transfer during multiple droplet impingement and spray cooling: Review and prospects for enhanced surfaces. *International Journal of Heat and Mass Transfer*, *178*, 121587. <https://doi.org/10.1016/j.ijheatmasstransfer.2021.121587>
- Schnell, G., Polley, C., Thomas, R., Bartling, S., Wagner, J., Springer, A., & Seitz, H. (2023). How droplets move on laser-structured surfaces: Determination of droplet adhesion forces on nano- and microstructured surfaces. *Journal of Colloid and Interface Science*, *630*, 951–964. <https://doi.org/10.1016/j.jcis.2022.10.091>
- Stratakis, E., Bonse, J., Heitz, J., Siegel, J., Tsididis, G., Skoulas, E., Papadopoulos, A., Mimidis, A., Joel, A. C., & Comanns, P. (2020). Laser engineering of biomimetic surfaces. *Materials Science and Engineering: R: Reports*, *141*, 100562. <https://doi.org/10.1016/j.mser.2020.100562>
- Zhou, S., Jiang, L., & Dong, Z. C. (2021). Bioinspired surface with superwettability for controllable liquid dynamics. *Advanced Materials Interfaces*, *8*(2), 2000824. <https://doi.org/10.1002/admi.202000824>
- Li, M., Li, C., Blackman, B. R., & Eduardo, S. (2022). Mimicking nature to control bio-material surface wetting and adhesion. *International Materials Reviews*, *67*(6), 658–681. <https://doi.org/10.1080/09506608.2021.1995112>
- Xu, J. K., Xiu, S. Y., Lian, Z. X., Yu, H. D., & Cao, J. J. (2022). Bioinspired materials for droplet manipulation: Principles, methods and applications. *Droplet*, *1*(1), 11–37. <https://doi.org/10.1002/dro.2.12>
- Ren, J. H., & Duan, F. (2021). Recent progress in experiments for sessile droplet wetting on structured surfaces. *Current Opinion in Colloid & Interface Science*, *53*, 101425. <https://doi.org/10.1016/j.cocis.2021.101425>
- Teodori, E., Moita, A. S., Moura, M., Pontes, P., Moreira, A., Bai, Y., Li, X., & Liu, Y. (2017). Application of bioinspired superhydrophobic surfaces in two-phase heat transfer experiments. *Journal of Bionic Engineering*, *14*(3), 506–519. [https://doi.org/10.1016/S1672-6529\(16\)60417-1](https://doi.org/10.1016/S1672-6529(16)60417-1)
- Merlen, A., & Brunet, P. (2009). Impact of drops on non-wetting biomimetic surfaces. *Journal of Bionic Engineering*, *6*(4), 330–334. [https://doi.org/10.1016/S1672-6529\(08\)60141-9](https://doi.org/10.1016/S1672-6529(08)60141-9)
- Wang, Y., Zhao, W. N., Han, M., Xu, J., & Tam, K. C. (2023). Biomimetic surface engineering for sustainable water harvesting systems. *Nature Water*, *1*(7), 587–601. <https://doi.org/10.1038/s44221-023-00109-1>
- Bhushan, B., & Jung, Y. C. (2011). Natural and biomimetic artificial surfaces for superhydrophobicity, self-cleaning, low adhesion, and drag reduction. *Progress in Materials Science*, *56*(1), 1–108. <https://doi.org/10.1016/j.pmatsci.2010.04.003>
- Jaggessar, A., Shahali, H., Mathew, A., & Yarlalagadda, P. (2017). Bio-mimicking nano and micro-structured surface fabrication for antibacterial properties in medical implants. *Journal of Nanobiotechnology*, *15*(1), 64. <https://doi.org/10.1186/s12951-017-0306-1>
- Wang, T., Huang, L., Liu, Y., Li, X., Liu, C., Handschuh-Wang, S., Xu, Y., Zhao, Y., & Tang, Y. (2020). Robust biomimetic hierarchical diamond architecture with a self-cleaning, antibacterial, and antibiofouling surface. *ACS Applied Materials & Interfaces*, *12*(21), 24432–24441. <https://doi.org/10.1021/acsami.0c02460>
- Kabi, P., Razdan, V., Roy, D., Bansal, L., Sahoo, S., Mukherjee, R., Chaudhuri, S., & Basu, S. (2021). Evaporation-induced alterations in Oscillation and flow characteristics of a sessile droplet on a rose-mimetic surface. *Soft Matter*, *17*(6), 1487–1496. <https://doi.org/10.1039/D0SM02106G>
- Gong, Y. X., Xu, J., & Buchanan, R. C. (2018). Surface roughness: A review of its measurement at micro-/nano-scale. *Physical Sciences Reviews*, *3*(1), 20170057. <https://doi.org/10.1515/psr-2017-0057>
- Bhushan, B. (2011). Biomimetics inspired surfaces for drag reduction and oleophobicity/philocity. *Beilstein Journal of Nanotechnology*, *2*(1), 66–84. <https://doi.org/10.3762/bjnano.2.9>
- Yang, Y., Li, X. J., Zheng, X., Chen, Z. Y., Zhou, Q. F., & Chen, Y. (2018). 3D-Printed biomimetic super-hydrophobic structure for microdroplet manipulation and oil/water separation. *Advanced Materials*, *30*(9), 1704912. <https://doi.org/10.1002/adma.201704912>
- Li, J., Feng, Q. X., Guo, N., Wang, F., Du, X., & Du, F. (2022). Preparation of a biomimetic superomniphobic hierarchical structure and analysis of droplet wettability. *Biosurface and Biotribology*, *8*(2), 129–139. <https://doi.org/10.1049/bsb2.12037>
- Günay, A. A., Kim, M. K., Yan, X., Miljkovic, N., & Sett, S. (2021). Droplet evaporation dynamics on microstructured biphilic, hydrophobic, and smooth surfaces. *Experiments in Fluids*, *62*, 1–14. <https://doi.org/10.1007/s00348-021-03242-3>
- Bhushan, B., Jung, Y. C., Niemietz, A., & Koch, K. (2009). Lotus-like biomimetic hierarchical structures developed by the self-assembly of tubular plant waxes. *Langmuir*, *25*(3), 1659–1666. <https://doi.org/10.1021/la802491k>
- Das, A., Polacchi, L., Courreges, C., Fouron, J. Y., Tournier-Couturier, L., Billon, L., & Luengo, G. S. (2024). Evaporative drying induced self-assembly of epicuticular wax: A biomimetic approach in tuning surface roughness. *Langmuir*, *40*(14), 7581–7594. <https://doi.org/10.1021/acs.langmuir.4c00205>
- Nosonovsky, M., & Bhushan, B. (2007). Biomimetic superhydrophobic surfaces: Multiscale approach. *Nano Letters*, *7*(9), 2633–2637. <https://doi.org/10.1021/nl071023f>
- Lin, H. P., & Chen, L. J. (2021). Direct observation of wetting behavior of water drops on single micro-scale roughness surfaces of Rose petal effect. *Journal of Colloid and Interface Science*, *603*, 539–549. <https://doi.org/10.1016/j.jcis.2021.06.132>
- Nosonovsky, M., & Bhushan, B. (2008). Biologically inspired surfaces: Broadening the scope of roughness. *Advanced Functional Materials*, *18*(6), 843–855. <https://doi.org/10.1002/adfm.200701195>

28. Li, C., Yang, J. J., He, W. J., Xiong, M. Y., Niu, X. S., Li, X. Y., & Yu, D. G. (2023). A review on fabrication and application of tunable hybrid micro–nano array surfaces. *Advanced Materials Interfaces*, 10(6), 2202160. <https://doi.org/10.1002/admi.202202160>
29. Park, J. E., Won, S., Cho, W., Kim, J. G., Jhang, S., Lee, J. G., & Wie, J. J. (2021). Fabrication and applications of stimuli-responsive micro/nanopillar arrays. *Journal of Polymer Science*, 59(14), 1491–1517. <https://doi.org/10.1002/pol.20210311>
30. Shahsavan, H., Arunbabu, D., & Zhao, B. (2012). Biomimetic modification of polymeric surfaces: A promising pathway for tuning of wetting and adhesion. *Macromolecular Materials and Engineering*, 297(8), 743–760. <https://doi.org/10.1002/mame.201200016>
31. Liang, W. Y., He, L., Wang, F. X., Yang, B., & Wang, Z. Q. (2017). A 3-D model for thermodynamic analysis of hierarchical structured superhydrophobic surfaces. *Colloids and Surfaces A: Physicochemical and Engineering Aspects*, 523, 98–105. <https://doi.org/10.1016/j.colsurfa.2017.04.001>
32. Luo, W. P., Yu, B., Xiao, D. B., Zhang, M., Wu, X. Z., & Li, G. X. (2018). Biomimetic superhydrophobic hollowed-out pyramid surface based on self-assembly. *Materials*, 11(5), 813. <https://doi.org/10.3390/ma11050813>
33. Okulova, N., Johansen, P., Christensen, L., & Taboryski, R. (2018). Effect of structure hierarchy for superhydrophobic polymer surfaces studied by droplet evaporation. *Nanomaterials*, 8(10), 831. <https://doi.org/10.3390/nano8100831>
34. Lee, J., Hwang, S. H., Yoon, S. S., & Khang, D. Y. (2019). Evaporation characteristics of water droplets in Cassie, Wenzel, and mixed States on superhydrophobic pillared Si surface. *Colloids and Surfaces A: Physicochemical and Engineering Aspects*, 562, 304–309. <https://doi.org/10.1016/j.colsurfa.2018.11.049>
35. Hu, A. J., & Liu, D. (2022). 3D simulation of micro droplet impact on the structured superhydrophobic surface. *International Journal of Multiphase Flow*, 147, 103887. <https://doi.org/10.1016/j.ijmultiphaseflow.2021.103887>
36. Zhang, Z. Y., Gu, Q. M., Jiang, W., Zhu, H., Xu, K., Ren, Y. P., & Xu, C. (2019). Achieving of bionic super-hydrophobicity by electrodepositing nano-Ni-pyramids on the picosecond laser-ablated micro-Cu-cone surface. *Surface and Coatings Technology*, 363, 170–178. <https://doi.org/10.1016/j.surfcoat.2019.02.037>
37. Li, Z. L., Li, W. W., Xun, M., & Yuan, M. C. (2023). WEDM one-step Preparation of miniature heat sink with superhydrophobic and efficient heat transfer performance. *The International Journal of Advanced Manufacturing Technology*, 127(3), 1873–1885. <https://doi.org/10.1007/s00170-023-11679-5>
38. Kim, S. J., Kim, D. H., Choi, S. H., Kim, W. Y., Kwon, S., & Cho, Y. T. (2020). Effect of surface pattern morphology on inducing superhydrophobicity. *Applied Surface Science*, 513, 145847. <https://doi.org/10.1016/j.apsusc.2020.145847>
39. Nasser, J., Lin, J. J., Zhang, L. S., & Sodano, H. A. (2020). Laser induced graphene printing of spatially controlled super-hydrophobic/hydrophilic surfaces. *Carbon*, 162, 570–578. <https://doi.org/10.1016/j.carbon.2020.03.002>
40. Li, R., Wang, Z. Y., He, L., Wang, B., Mao, H. Y., & Yu, M. L. (2024). Characterization of the effect of fractal micro-protrusion and heat on the wettability behavior on chips in medical MEMS. *Materials Today Communications*, 39, 108547. <https://doi.org/10.1016/j.mtcomm.2024.108547>
41. Hao, C. L., Liu, Y. H., Chen, X. M., Li, J., Zhang, M., Zhao, Y. H., & Wang, Z. K. (2016). Bioinspired interfacial materials with enhanced drop mobility: From fundamentals to multifunctional applications. *Small (Weinheim an Der Bergstrasse, Germany)*, 12(14), 1825–1839. <https://doi.org/10.1002/smll.201503060>
42. Yang, X., Zhang, W., Qin, X., Cui, M., Guo, Y., Wang, T., Wang, K., Shi, Z., Zhang, C., Li, W., & Wang, Z. (2022). Recent progress on bioinspired antibacterial surfaces for biomedical application. *Biomimetics*, 7(3), 88. <https://doi.org/10.3390/biomimetics7030088>
43. Zhang, B. P., Xu, W. H., Peng, L., Li, Y. C., Zhang, W., & Wang, Z. K. (2024). Nature-inspired interfacial engineering for energy harvesting. *Nature Reviews Electrical Engineering*, 1, 218–233. <https://doi.org/10.1038/s44287-024-00029-6>
44. Mitra, S. K., & Chakraborty, S. (2012). *Microfluidics and Nanofluidics Handbook: Fabrication, Implementation, and Applications*. Taylor & Francis.
45. Wenzel, R. N. (1936). Resistance of solid surfaces to wetting by water. *Industrial & Engineering Chemistry*, 28(8), 988–994. <https://doi.org/10.1021/ie50320a024>
46. Van Oss, C. J. (2006). *Interfacial Forces in Aqueous Media*. CRC.
47. Berthier, J. (2012). *Micro-drops and Digital Microfluidics*. William Andrew.
48. Pan, Z. H., Weibel, J. A., & Garimella, S. V. (2020). Transport mechanisms during water droplet evaporation on heated substrates of different wettability. *International Journal of Heat and Mass Transfer*, 152, 119524. <https://doi.org/10.1016/j.ijheatmasstransfer.2020.119524>

**Publisher's Note** Springer Nature remains neutral with regard to jurisdictional claims in published maps and institutional affiliations.